JOURNAL OF MATERIALS SCIENCE 35 (2000) 3497–3504

Fracture behavior of notched unidirectional Si-Ti-C-O/BMAS composite

S. OCHIAI*, I. OKUMURA, M. TANAKA, M. HOJO
Mesoscopic Materials Research Center, Kyoto University, Sakyo-ku, Kyoto 606-8501, Japan
E-mail: ochiai@mech.kyoto-u.ac.jp

M. SATO, M. TAMURA, Y. KOHTOKU, T. YAMAMURA
Corporate Research and Development, Ube Industries Ltd, Ube, Yamaguchi 755-8633, Japan

Experimental and modeling studies on tensile fracture behavior of notched unidirectional Si-Ti-C-O (Tyranno fiber) reinforced BMAS (barium magnesium aluminosilicate) glass matrix composite were carried out. The longitudinal crack arose at the tip of the transverse notch before overall fracture. The critical energy release rate around at initiation of the longitudinal cracking was estimated to be nearly 100 J/m^2 by application of the present model to the experimentally observed relation between the stress of the composite in the very early stage of longitudinal cracking and the notch size. The notched strength was higher than that predicted by the fracture mechanical criterion due to the blunting arising from the premature longitudinal cracking, but it was lower than that predicted by the net stress criterion due to the constraint effect arising from the bridging of the fibers and the spalling of the segmented matrix into the longitudinal crack.

1. Introduction

Glass-ceramics such as LAS (lithium aluminosilicate), CAS (calcium aluminosilicate), MAS (magnesium aluminosilicate) and BMAS (barium magnesium aluminosilicate) have an advantage over ceramics as a matrix material for fiber-composites in the fabrication process on the point that the composites can be easily consolidated at lower temperatures and then the matrix can be converted to crystallized glass-ceramic to achieve high temperature stability. Concerning the mechanical property, it has been shown that the glass-ceramic matrix composites have high specific strength, toughness and high-temperature oxidation resistance [1–8].

Kumar and Knowles [4] have shown that a common feature of Si-C-O (Nicalon) fiber reinforced glass-ceramic matrix composites is the presence of thin layer of carbon at the interface. Tamura *et al.* [3] have also shown that carbon-rich layer exists at the interface in the Si-Ti-C-O (Tyranno fiber)/BMAS composite. Such a carbon or carbon-rich layer, giving limited bonding strength, promotes crack deflection and fiber pull-out [5–7], which results in a flaw tolerable or notch-insensitive behavior of composite over the unreinforced matrix [8].

In the present work, tensile fracture behavior of the notched Si-Ti-C-O fiber-reinforced BMAS matrix composite developed at Ube Industries [3] was studied at room temperature. In Section 3, the experimentally observed features of this composite that (1) a longitudinal cracking occurs at the tip of the transverse notch and (2) the notched strength is not sensitive but not insensitive to the transverse notch, will be presented. In Section 4, a simple model will be presented, with which the critical energy release rate for longitudinal cracking will be estimated for the feature (1) and the reason for the feature (2) will be accounted for.

2. Experimental procedure

The Si-Ti-C-O (Tyranno fiber, F-grade)/BMAS composite samples were fabricated at Ube Industries by the method shown in Ref. [3]. The volume fraction of the fiber V_f was 0.5.

The single-edge-notched specimens were used for tensile test. The width W, thickness T and the gauge length were 5, 1 and 150 mm, respectively. The relative notch length (c/W where c is the notch length) was varied from zero to 0.5. The radius of the notch tip was made to be 50 μm with a saw. In order to avoid the damage of the specimens in the grips, GFRP (glass fiber-reinforced plastics) tabs were pasted on both ends of the specimens. Tensile test was carried out at room temperature at a cross-head speed of 8.3×10^{-3} mm/s. The fracture surface was observed with a scanning electron microscope.

3. Experimental results

3.1. Longitudinal cracking

In all notched specimens, longitudinal cracking, more or less, occurred at the tip of the transverse notch prior to

* Author to whom all correspondence should be addressed.

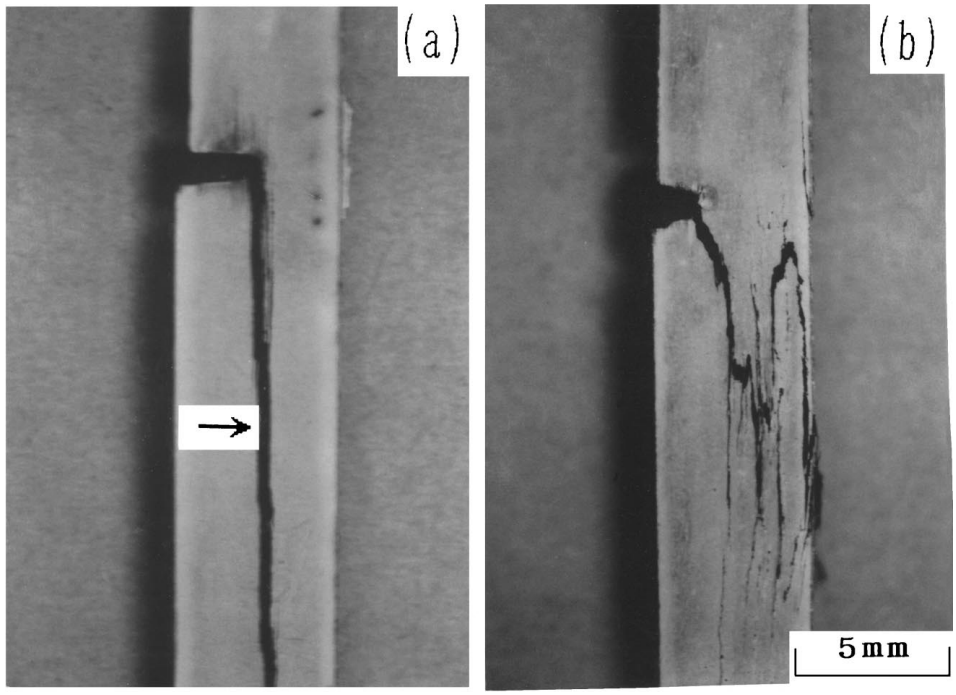

Figure 1 Appearance of the specimens during tensile test showing occurrence of the longitudinal cracking for (a) long and (b) short distances. Some specimens showed (a) and others (b) prior to the overall fracture. The fracture surface of the longitudinally cracked portion indicated by the arrow in (a) will be shown later in Fig. 3.

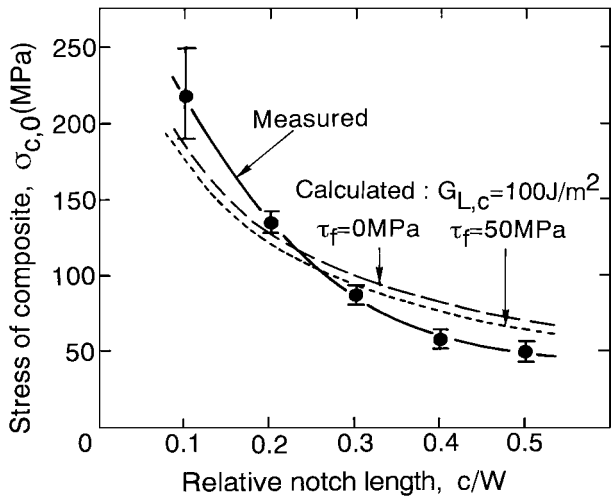

Figure 2 Measured stress of the composite $\sigma_{c,0}$ at which the length of the longitudinal cracking reaches 100 μm plotted against relative notch length c/W. The closed circles show the average of 2 specimens. The broken and dotted curves show the calculated $\sigma_{c,0}$-c/W relations for $\tau_f = 0$ and 50 MPa, respectively, in which the critical energy release rate $G_{L,c}$ is taken to be 100 J/m^2.

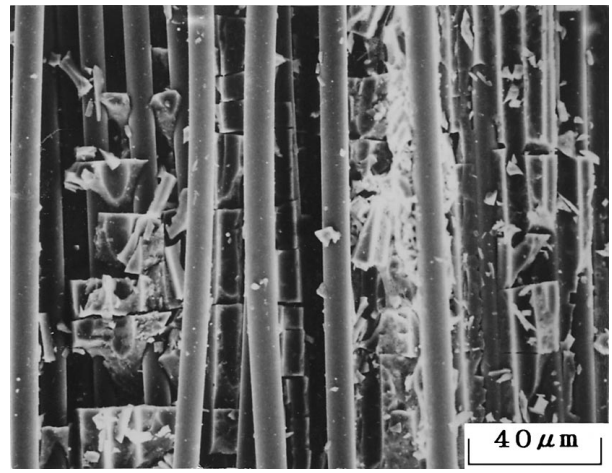

Figure 3 Surface of the longitudinal crack indicated by the arrow in Fig. 1a.

the overall fracture. Fig. 1(a) shows the case where the longitudinal cracking occurred for long distance nearly up to the end of specimen and (b) the case where it occurred for short distance, followed by the complex progress of overall fracture.

As it was difficult to estimate experimentally the exact composite stress at initiation of the longitudinal crack, the stress of composite at which the length of the longitudinal cracking reaches around 100 μm was measured. Hereafter such a stress of composite around at initiation is described as $\sigma_{c,0}$. The experimental result for the variation of $\sigma_{c,0}$ with the relative notch length c/W is shown in Fig. 2. Evidently, the values of $\sigma_{c,0}$ decreases with increasing c/W.

Fig. 3 shows the surface of the longitudinal crack indicated by the arrow in Fig. 1a. The interfacial debonding between fiber and matrix, and segmentation and spalling of the matrix are found. It is suggested that the segmented matrix spallen into the longitudinal crack acts to generate frictional stress between the crack surfaces. Fig. 4 shows the bridging of the fibers observed during progress of the longitudinal crack. It is suggested that the bridging acts to give the constraint effect and to retard the growth of longitudinal cracking.

3.2. Notched strength and fracture surface

As shown in Fig. 1, the notch does not propagate into transverse direction due to the growth of the

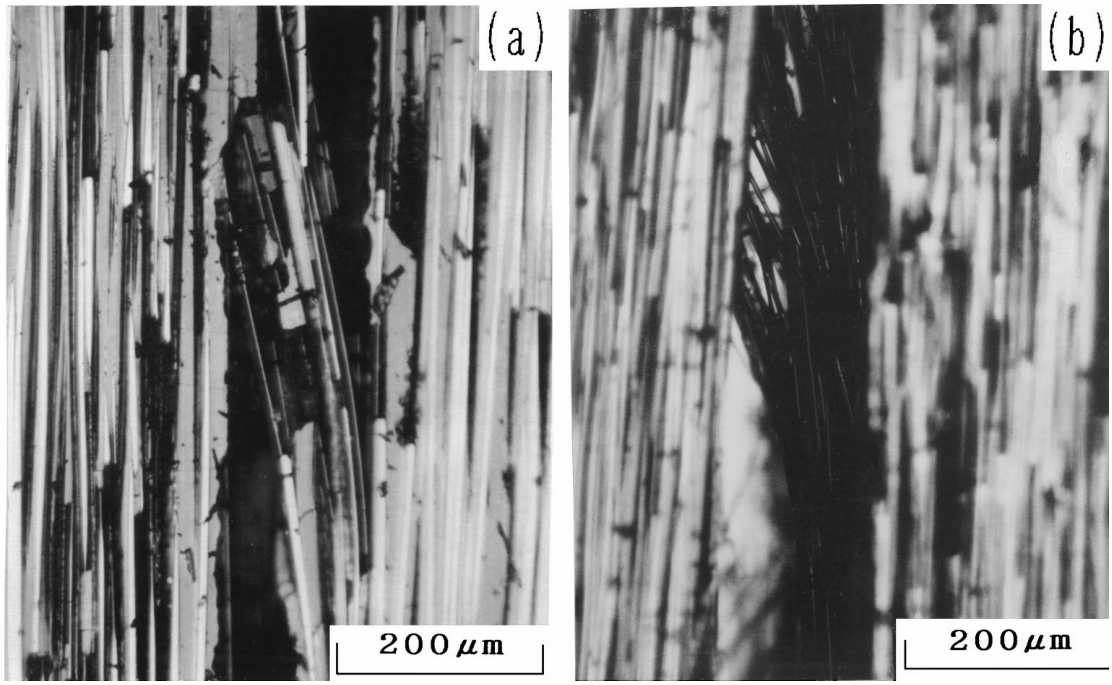

Figure 4 Bridging of the fibers observed during the growth of the longitudinal crack.

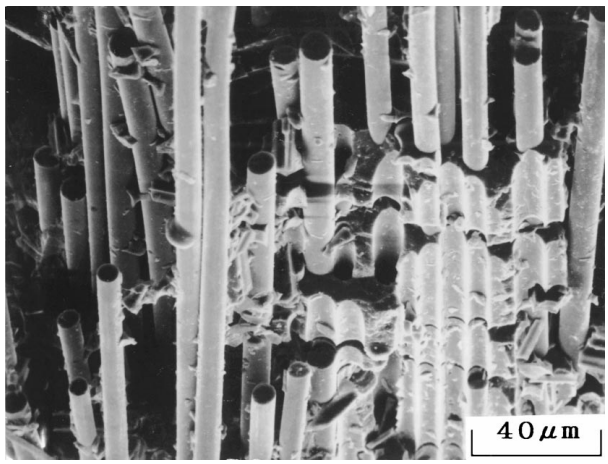

Figure 5 Fracture surface of the notched specimen, showing long pull-out of fibers.

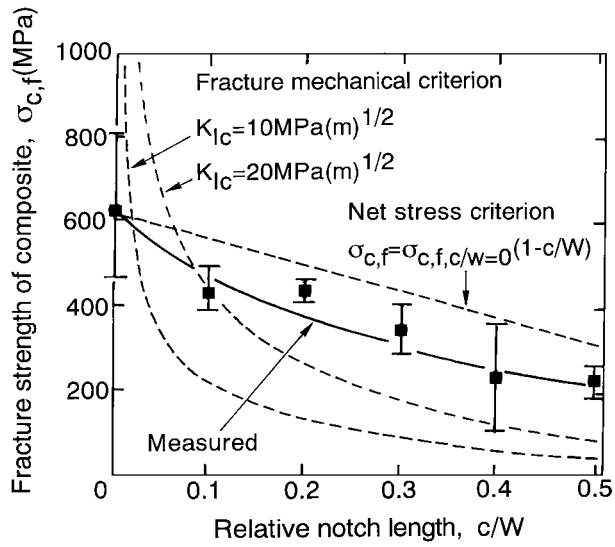

Figure 6 Measured fracture strength $\sigma_{c,f}$ plotted against c/W. The closed squares show the average and the error bars show the maximum and minimum of 5 specimens for $c/W = 0$ and those of 3 specimens for $c/W = 0.1$ to 0.5. If the composite is assumed to be completely notch-insensitive, namely if the premature longitudinal cracking occurs over the entire gage length and there is no interaction between the separated portions, the strength is expected to decrease with increasing c/W as shown with broken line shown by $\sigma_{c,f} = \sigma_{c,f,c/W=0}\,(1 - c/W)$ (net stress criterion) where $\sigma_{c,f,c/W=0}$ is the strength of the unnotched specimen. If the composite is assumed to be completely notch sensitive, namely if no premature longitudinal cracking occurs, the strength is expected to decrease with increasing c/W as shown with the broken curves for $K_{Ic} = 10$ and 20 MPa(m)$^{1/2}$ for instance (fracture mechanical criterion). The strength of the present composite is in the intermediate range between the net stress- and fracture mechanical criteria.

longitudinal crack prior to the overall fracture. This can be attributed to the weak interface between fiber and matrix, which is demonstrated by the interfacial debonding in Fig. 3 and by the long pull-out of the fibers in the final fracture surface in Fig. 5.

Fig. 6 shows the measured fracture strength $\sigma_{c,f}$ plotted against c/W. The closed squares show the average measured values and the error bars show the maximum and minim measured values among 5 specimens for $c/W = 0$ (unnotched) and among 3 specimens for $c/W = 0.1$ to 0.5. If the composite is assumed to be completely notch-insensitive, namely if the premature longitudinal cracking occurs over the entire gage length and no interaction between the separated two portions, the strength is expected to decrease with increasing c/W as shown with the broken line indicated by $\sigma_{c,f} = \sigma_{c,f,c/W=0}\ (1 - c/W)$ (net stress criterion) where $\sigma_{c,f,c/W=0}$ is the strength of the unnotched specimen. If the composite is assumed to be completely notch sensitive, namely if no premature longitudinal cracking occurs and the linear elastic fracture mechanical criterion can be applied, the strength is expected to decrease sharply with increasing c/W as shown with the broken curves for $K_{Ic} = 10$ and 20 MPa (m)$^{1/2}$ for instance. The strength of the present composite is in the

intermediate range between the net stress- and fracture mechanical criteria.

4. Modeling and discussion

4.1. Simplified modeling for calculation of energy release rate for longitudinal cracking and of stress distribution under existence of the longitudinal cracking

A simplified model for calculation of the energy release rate for the longitudinal cracking to arise and of the variation of the stress distribution with progress of the longitudinal cracking is presented in 4.1. This model is applied to the experimental results, and the critical energy release rate for the very early stage of longitudinal cracking is estimated in 4.2. The reason, why the notched strength was in the intermediate range between the fracture mechanical- and net stress criteria, is accounted for in 4.3 from the calculated stress distribution in the composite with longitudinal cracking.

4.1.1. Simplification

The longitudinal cracking is accompanied with multiple breakage of matrix, debonding of interface, spalling of the segmented matrix into the crack and bridging of fibers as shown above. The description of this phenomenon requires the three-dimensional analysis containing such phenomena, which, however, cannot be solved in a rigid manner at present. From the practical viewpoint, it is needed to develop the estimation method, which may be rough but can describe outlines quickly. One of the candidates for this aim is to use the concept and mathematical technique of the shear lag analysis method [10–17]. In this work, as one step, a simplified two-dimensional model using the shear lag analysis modified to be applicable to ceramic matrix composites [14–17] is presented.

The composite with a width W and a thickness T was regarded to be composed of mini-composite-elements with a width D. The element at the left side is numbered as "1", the next one as "2", and then "3", "4", ... to "N", as shown in Fig. 7. "1" to "Nc" elements are cut due to the introduction of the notch. The width, cross-sectional area, Young's modulus and shear modulus of each element are given by d, $A(=\mathrm{TD})$, E_c and G_c, respectively.

When the applied stress exceeds the critical value, the longitudinal cracking occurs at the interface between "Nc" and "Nc + 1" elements. In this work, the longitudinal cracking was judged to occur when the length d of the crack reached 100 μm, as has been stated in Section 3. Then the situation for $d > 0$ is considered. We divide the specimen into two regions for convenience: Regions A and B in which the longitudinal cracking has not occurred and it has occurred, respectively. Noting the distance in longitudinal direction from the notch as x, Regions A and B cover $d \leq x$ and $0 \leq x \leq d$, respectively. In Region B, the bridging of fibers and spalling of segmented matrix into the crack are regarded to act as the cause of the frictional shear

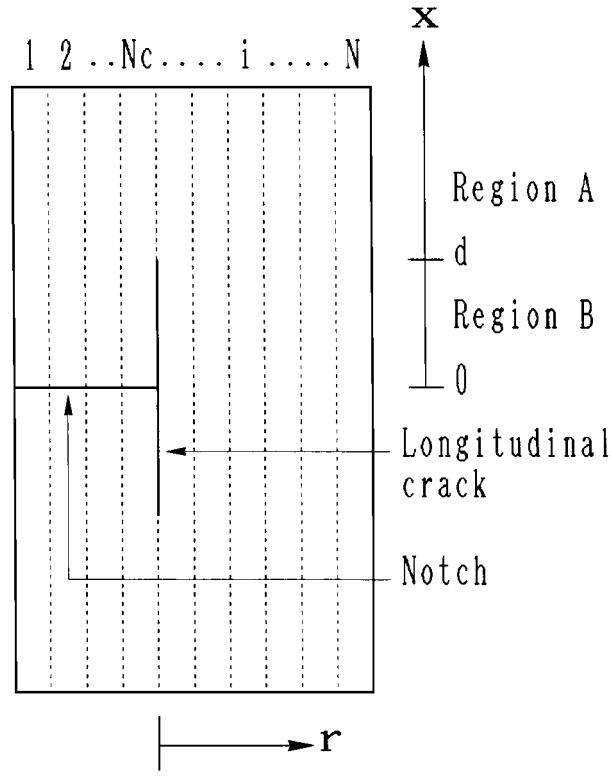

Figure 7 Two-dimensional modeling for calculation. The composite was regarded to be composed of many mini-composite-elements, which were numbered 1 to N from left to right sides. The region, where the longitudinal cracking has not occurred, is called as Region A, and the region where it has occurred by d in length as Region B.

stress τ_f at the "Nc"/"Nc + 1" interface, to a first approximation.

4.1.2. Equations for stress equilibrium

The displacement of the "i" element is defined as u_i and that of the interface between "i" and "$i + 1$" elements as $u_{i/i+1}$, which are a function of x. In Region A, the exerted shear stress at the interface between "i" and "$i + 1$" elements, $\tau_{i/(i+1)}$, is given by the Dow's method [18] as follows.

$$\tau_{i/(i+1)} = (u_{i+1} - u_{i/i+1})\left\{\frac{G_c}{D/2}\right\}$$

$$= (u_{i/i+1} - u_i)\left\{\frac{G_c}{D/2}\right\} \quad (1)$$

Eliminating $u_{i/i+1}$ in Equation (1), $\tau_{i/(i+1)}$ is expressed as

$$\tau_{i/(i+1)} = \left(\frac{G_c}{D}\right)(u_{i+1} - u_i) \quad (2)$$

The interfacial shear stress between "Nc" and "Nc + 1" elements, $\tau_{Nc/(Nc+1)}$, in Region A, is expressed by

$$\tau_{Nc/(Nc+1)} = \left(\frac{G_c}{D}\right)(u_{Nc+1} - u_{Nc}) \quad (3)$$

In Region B, the interface between "Nc"- and "Nc + 1"-elements is broken but the frictional shear stress τ_f

(assumed to be constant to a first approximation) is exerted so that $\tau_{Nc}/(Nc+1)$ for $0 \le x \le d$ is given by

$$\tau_{Nc/(Nc+1)} = \beta\tau_f \tag{4}$$

where β is the parameter indicating the direction of the frictional shear stress, being 1 and -1 when $u^B_{Nc+1} - u^B_{Nc} > 0$ and <0, respectively.

The shear stresses at the left and right side surfaces of "1" and "N" elements are zero, respectively. From these situations, the equations to solve u_i for Regions A and B for $i = 1$ to N are given as follows.

Region A:

$$DE_c\left(\frac{d^2u_1^A}{dx^2}\right) + \left(\frac{G_c}{D}\right)(u_2^A - u_1^A) = 0 \tag{5}$$

$$DE_c\left(\frac{d^2u_i^A}{dx^2}\right) + \left(\frac{G_c}{D}\right)(u_{i+1}^A - 2u_i^A + u_{i-1}^A) = 0 \quad (i = 2 \text{ to } N-1) \tag{6}$$

$$DE_c\left(\frac{d^2u_N^A}{dx^2}\right) - \left(\frac{G_c}{D}\right)(u_N^A - u_{N-1}^A) = 0 \tag{7}$$

Region B:

$$DE_c\left(\frac{d^2u_1^B}{dx^2}\right) + \left(\frac{G_c}{D}\right)(u_2^B - u_1^B) = 0 \tag{8}$$

$$DE_c\left(\frac{d^2u_i^B}{dx^2}\right) + \left(\frac{G_c}{D}\right)(u_{i+1}^B - 2u_i^B + u_{i-1}^B) = 0 \quad (i = 2 \text{ to } Nc-1) \tag{9}$$

$$DE_c\left(\frac{d^2u_{Nc}^B}{dx^2}\right) - \left(\frac{G_c}{D}\right)(u_{Nc}^B - u_{Nc-1}^B) + \beta\tau_f = 0 \tag{10}$$

$$DE_c\left(\frac{d^2u_{Nc+1}^B}{dx^2}\right) + \left(\frac{G_c}{D}\right)(u_{Nc+2}^B - u_{Nc+1}^B) - \beta\tau_f = 0 \tag{11}$$

$$DE_c\left(\frac{d^2u_i^B}{dx^2}\right) + \left(\frac{G_c}{D}\right)(u_{i+1}^B - 2u_i^B + u_{i-1}^B) = 0 \quad (i = Nc+2 \text{ to } N-1) \tag{12}$$

$$DE_c\left(\frac{d^2u_N^B}{dx^2}\right) - \left(\frac{G_c}{D}\right)(u_N^B - u_{N-1}^B) = 0 \tag{13}$$

where the superscripts A and B for u_i refer to Regions A and B, respectively.

The Equations 5 to 13 were solved by using the mathematical technique shown elsewhere [16, 17]. The derived general solution of u_i ($i = 1$ to N) for Regions A and B are shown in Appendix 1. The A_j and C_j ($i = 1$ to $2N$) in Equations A1–A3 are unknown constants which can be solved by the following boundary conditions.

4.1.3. Boundary conditions

Noting the applied stress as σ_c, the boundary conditions are given as follows.

(i) At $x = 0$, the displacements of the uncut elements ("$Nc+1$" to "N") are zero; $(u_i^B)_{x=0} = 0$ ($i = Nc+1$ to N), and the strains of the cut elements are zero; $(du_i^B/dx)_{x=0} = 0$ ($i = 1$ to Nc).

(ii) At $x = d$, the displacements and strains are continuous; $(u_i^A)_{x=d} = (u_i^B)_{x=d}$ and $(du_i^A/dx)_{x=d} = (du_i^B/dx)_{x=d}$ ($i = 1$ to N).

(iii) At $x = \infty$, the strain of each element is equal to σ_c/E_c ($i = 1$ to N).

4.1.4. Calculation of stress distribution and energy release rate for longitudinal cracking

When A_j and C_j-values are determined by the boundary conditions mentioned above, the stress of each element at any x is calculated by $E_c\,(du_i/dx)$. Also the shear stress is calculated by Equations 2 to 4.

When the area of the cracked interface increases from $S(=Td)$ to $S + \Delta S\,\{=T(d+\Delta d)\}$ under an applied load $P(=\sigma_c WT)$, the energy release rate for the longitudinal cracking is given by

$$G_L = \lim_{\Delta d \to 0}\left[\frac{(W_p - \Delta U_e)}{T\,\Delta d}\right] \tag{14}$$

where W_p is the work done by the applied load and ΔU_e is the difference in internal energy due to the growth of the debonding by ΔS in area. The details to calculate Equation 14 is presented in Appendix 2.

4.2. Energy release rate for longitudinal cracking around at initiation

Following values were used for calculation; $W = 5$ mm, $c/W = 0.1$ to 0.5 in step of 0.1, $E_c = 130$ GPa, $G_c = 52$ GPa and $\tau_f = 0$ to 50 MPa. Fig. 8 shows variations of the energy release rate G_L for the longitudinal cracking at $d = 100\ \mu$m at the Nc/(Nc + 1) interface as

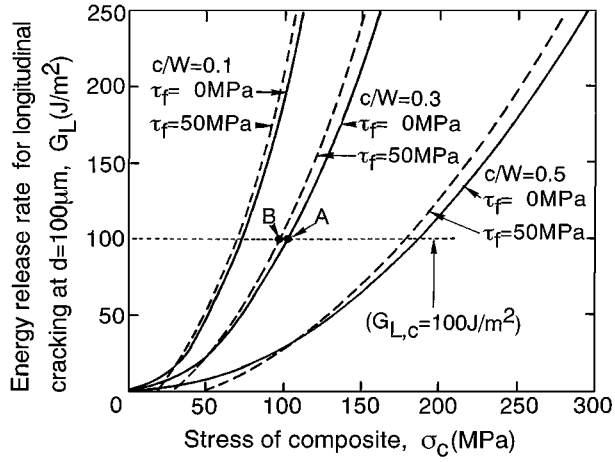

Figure 8 Variations of the energy release rate G_L for the longitudinal cracking at $d = 100\ \mu$m at the Nc/(Nc + 1) interface as a function of applied stress of composite, σ_c, for $c/W = 0.1$, 0.3 and 0.5 as an example. In the calculation, τ_f was varied from 0 to 50 MPa and it was found that the $G_L - \sigma_c$ curves were not much affected by the value of τ_f, so that the calculation results only for $\tau_f = 0$ and 50 MPa are representatively presented in this figure. If the critical energy release rate for the longitudinal cracking, $G_{L,c}$, is taken to be 100 J/m^2, the cracking for $c/W = 0.3$ occurs at A and B for $\tau_f = 0$ and 50 MPa, respectively.

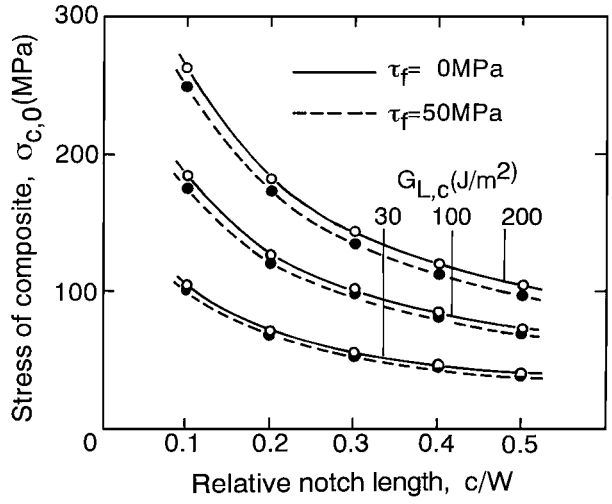

Figure 9 Calculated variations of the stress of composite $\sigma_{c,0}$ at $d =$ 100 μm of the longitudinal cracking as a function of c/W for the critical energy release rate $G_{L,c} = 30$, 100 and 200 J/m^2.

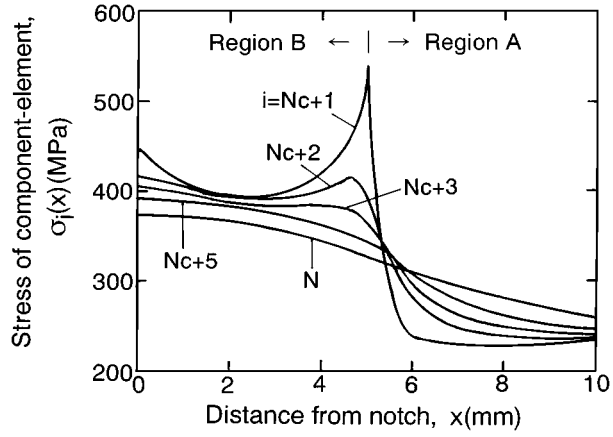

Figure 10 Distribution of the tensile stress σ_i (x) in the "i" component-element ($i = \mathrm{Nc}+1$ to N) along x axis for an example of $c/W = 0.4$, $\sigma_c = 236$ MPa, $\tau_f = 20$ MPa and $d = 5$ mm.

a function of applied stress of composite, σ_c. As the calculated $G_L - \sigma_c$ curves for $\tau_f = 10$ to 40 MPa were within the range for $\tau_f = 0$ and 50 MPa, only the results for $\tau_f = 0$ and 50 MPa are presented in this figure. Evidently, G_L-value increases with increasing c/W at any σ_c, indicating that the larger the notch size, the higher becomes the energy release rate and hence the lower becomes the stress of composite around at initiation.

When a critical energy release rate, $G_{L,c}$, is given, the stress of composite around at initiation of the longitudinal cracking, $\sigma_{c,0}$, can be known as the stress satisfying $G_L = G_{L,c}$ in the $G_L - \sigma_c$ curves in Fig. 8. For instance, if $G_{L,c}$ is assumed to be 100 J/m^2, the $\sigma_{c,0}$-values for $\tau_f = 0$ and 50 MPa in the case of $c/W = 0.3$ are known from A and B, respectively. Fig. 9 shows thus calculated $\sigma_{c,0}$-c/W relations for the assumed values of $G_{L,c} = 30$, 100 and 200 J/m^2. The difference in $\sigma_{c,0}$ due to the difference in τ_f is small.

The result stated above suggests that the approximate $G_{L,c}$-value can be estimated by the curve-fitting to the experimentally observed $\sigma_{c,0}$-c/W curve even though τ_f-value is unknown. In the present composite, when $G_{L,c}$ is taken to be 100 J/m^2, the experimental results could be described fairly well, as shown in Fig. 2. In this way, the critical energy release rate for longitudinal cracking in the very early stage ($d = 100$ μm) or around at initiation of the present composite was identified to be around 100 J/m^2 to a first approximation.

The G_L-value is not sensitive to τ_f-value only for the very early stage. Even if τ_f-value is assumed to remain constant for any d, the G_L-value varies with d as similarly as the debonding between fiber and matrix in unidirectional fiber-reinforced composites [15–17]. Therefore, the present method to estimate $G_{L,c}$ is limited only to the early stage of cracking. In the practical cracking process, the value of τ_f is considered to change with increasing length of the longitudinal crack due to the change in extent of the bridging of fibers and the spallings of the segmented matrix into the crack. Thus the energy release rate is expected to be given as a function of the crack length, which shall be studied as the next work.

4.3. Notched strength

As shown in 3.2, the notched strength of the present composite was lower than that predicted by the net stress criterion but higher than that predicted by the fracture mechanical criterion. Namely the notched strength was not insensitive to the notch in spite of the premature longitudinal cracking but not so sensitive as in the case of no premature cracking. Such a behavior can be accounted for as follows.

Fig. 10 shows the distribution of the tensile stress σ_i (x) in the "i" component-element ($i = \mathrm{Nc}+1$ to N) for an example of $c/W = 0.4$, $\sigma_c = 236$ MPa, $\tau_f = 20$ MPa and $d = 5$ mm. As the length of the longitudinal crack is different from specimen to specimen, the case of $d = 5$ mm is taken as an example. In Region B in which the longitudinal crack has occurred (Fig. 7), the stress level decreases with increasing i (corresponding to the transverse distance from the notch, r, in Fig. 7) at any x, while, in Region A in which the longitudinal crack has not occurred, the stress level, roughly speaking, increases with increasing $i(r)$. Also the stress of "Nc + 1" and "Nc + 2" elements have two extremes at $x = 0$ and d. Especially, the extreme at $x = d$ of "Nc + 1" element is very high. In this way, the stress is concentrated especially for the "Nc + 1" element in Region B while no such stress concentration arises if the longitudinal crack occurs entirely the length and no interaction occurs between the separated two portions (corresponding to $\tau_f = 0$ and $d =$ infinite in this model).

In this way, the stress distribution of the "Nc + 1" element can be taken as the representative to express the stress concentration. Following three cases were taken up and the extent of stress concentration of "Nc + 1" element was compared to each other; case (A) in which the premature longitudinal cracking is assumed not to occur, corresponding to the notch sensitive situation where the notched strength can be described by the fracture mechanical criterion; case (B) in which the premature longitudinal crack is assumed to have occurred for the length of 2, 5 and 8 mm under the condition of $\tau_f = 20$ MPa, corresponding to the situation where the notched strength can be higher than that for case (A) but lower than that for case (C) below, as in the present specimens; and case (C) in which the premature

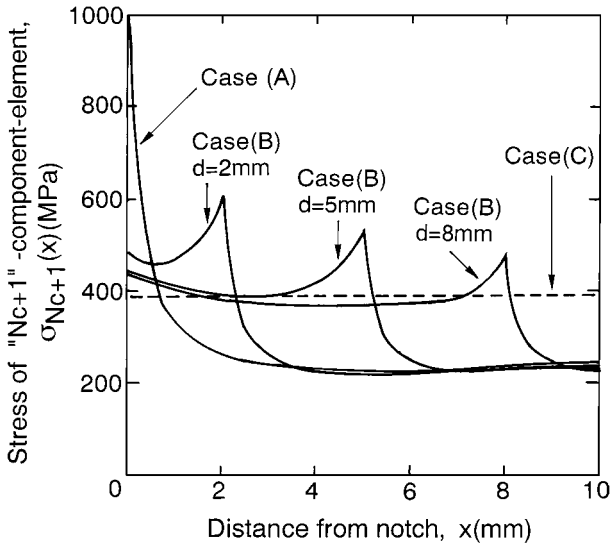

Figure 11 Distribution of tensile stress σ_{Nc+1} in the "Nc + 1" component-element along x axis calculated for cases (A), (B) and (C) for an example of $c/W = 0.4$ and $\sigma_c = 236$ MPa.

longitudinal cracking is assumed to have occurred entirely the specimen length and no interaction occurs between the separated portions ($\tau_f = 0$), corresponding to the case where the notched strength can be given by the net stress criterion.

Fig. 11 shows the calculation results. In case (A), the stress near the notch tip is very high. The highest stress level for case (B) is intermediate between the highest stress levels for cases (A) and (C). In this way, the higher strength of the present specimens than that predicted by the fracture mechanical criterion can be attributed to the premature longitudinal cracking, which reduces the stress concentration (blunting), and the lower strength than that predicted by the net stress criterion can be attributed to the occurrence of the stress concentration due to the existence of the frictional stress arising from the bridging of the fibers and spalling of the matrix segments.

There was the tendency in the calculation result that the larger the d, the lower becomes the stress concentration at $x = d$. The experimentally observed tendency, that the notched strength is high when the specimen fractures after large progress of the premature longitudinal cracking, might be attributed partly to such a dependency of the length of the premature longitudinal cracking on the blunting effect.

5. Conclusions

Tensile fracture behavior of notched unidirectional Si-Ti-C-O /BMAS composite was studied experimentally. To account for the experimental results, a simple model using the shear lag analysis was applied. Main results are summarized as follows.

(1) The longitudinal crack arose at the tip of the transverse notch before overall fracture.

(2) From the application of the present model to the experimentally observed relation between the stress of the composite in the early stage of longitudinal cracking and the transverse notch size, the critical energy release rate for the longitudinal cracking around at initiation was estimated to be nearly 100 J/m^2.

(3) The notched strength was higher than that predicted by the fracture mechanical criterion due to the blunting arising from the premature longitudinal cracking, but, it was lower than that predicted by the net stress criterion due to the constraint effect arising from the bridging of the fibers and the spalling of the segmented matrix into the longitudinal crack.

Appendix 1: General solutions of u_i

The general solution of u_i ($i = 1$ to N) for Regions A and B can be expressed as follows.

Region A:

$$u_i^{\mathrm{A}} = \sum_{j=1}^{2(N-1)} A_j B_{i,j} \exp(k_j x) + A_{2N-1} x + A_{2N} \quad (i = 1 \text{ to } N) \quad \text{(A1)}$$

Region B:

$$u_i^{\mathrm{B}} = \sum_{j=1}^{2(\mathrm{Nc}-1)} C_j D_{i,j} \exp(v_j x) + C_{2\mathrm{Nc}-1} x + C_{2\mathrm{Nc}} - \left\{ \frac{1}{DE_c} \right\} \frac{\beta \tau_f x^2}{2Nc} + X_i \beta \tau_f \quad (i = 1 \text{ to Nc}) \quad \text{(A2)}$$

$$u_i^{\mathrm{B}} = \sum_{j=2\mathrm{Nc}+1}^{2(N-1)} C_j D_{i,j} \exp(v_j x) + C_{2N-1} x + C_{2N} + \left\{ \frac{1}{DE_c} \right\} \frac{\beta \tau_f x^2}{2(N - Nc)} + Y_i \beta \tau_f \quad (i = \mathrm{Nc} + 1 \text{ to } N) \quad \text{(A3)}$$

where A_j's and C_j's ($j = 1$ to $2N$) are the unknown constants to be solved from the boundary conditions. k_j's ($j = 1$ to $2N - 2$), v_j's ($i = 1$ to $2N - 2$), $B_{i,j}$'s ($i = 1$ to N, $j = 1$ to $2N - 2$), $D_{i,j}$'s ($i = 1$ to N, $j = 1$ to $2N - 2$), X_i ($i = 1$ to Nc) and Y_i ($i = \mathrm{Nc} + 1$ to N) are mathematically determined constants and β is the direction parameter of the frictional shear stress, which is given by -1 in the present configuration, since $u_{Nc+1} - u_{Nc} < 0$ in Region B.

Appendix 2: Calculation method of energy release rate for longitudinal cracking

Noting the A_{2N}-values for the longitudinal crack areas $S + \Delta S$ and S as $A_{2N}(S + \Delta S)$ and $A_{2N}(S)$, respectively, the difference in the displacement at infinity is expressed by $A_{2N}(S + \Delta S) - A_{2N}(S)$ from the boundary condition for $x = \infty$ mentioned in 4.1 (C). As the composite deforms for both x and $-x$ directions, the work done by the applied load P, W_p, is given by

$$W_p = 2P\{A_{2N}(S + \Delta S) - A_{2N}(S)\} \quad \text{(A4)}$$

The difference in internal energy ΔU_e is given by

$$\Delta U_e = (\Delta U_E + \Delta U_G) \tag{A5}$$

where ΔU_E and ΔU_G are the differences in tensile and shear strain energies before and after the growth of longitudinal crack by ΔS in area, respectively, which can be calculated in a following manner. Noting the displacement of the "i" element for the cracked areas for S and $S + \Delta S$ as $u_i(S)$ and $u_i(S + \Delta S)$, respectively, the difference in internal energy $\Delta U_{E,i}$ in the "i" element due to the increase in the cracked area from S to $S + \Delta S$ is expressed as,

$$\Delta_{E,i} = \left(\frac{E_c DT}{2}\right)\left[\int_{-\infty}^{\infty}\left\{\frac{du_i(S+\Delta S)}{dx}\right\}^2 - \left\{\frac{du_i(S)}{dx}\right\}^2\right]dx \tag{A6}$$

Substituting Equations (A1), (A2) and (A3) whose constants A_j ($j = 1$ to $2N$) and C_j ($j = 1$ to $2N$) are determined by the boundary conditions given in 4.1(C) into Equation (A6), $\Delta U_{E,i}$ was calculated, from whose summation for $i = 1$ to N, the ΔU_E-value was calculated.

In the present simplified model, the shear strains in the left and right halves of "i" element are treated to be equal to $\tau_{(i-1)/i}/G_i$ and $\tau_{i/(i+1)}/G_i$. The shear strain energy of the "i" element is, therefore, given by the sum of the energies of the left and right halves. Thus, the difference in shear strain energy $\Delta U_{G,i}$ of the i element before and after the growth of longitudinal crack from S to $S + \Delta S$ in area is given by

$$\begin{aligned}\Delta U_{G,i} = \left(\frac{1}{2}\right)\left\{\frac{DT}{(2G_c)}\right\}\int_{-\infty}^{\infty}\big[&\{\tau_{i-1/i}(S+\Delta S)\}^2 \\ &- \{\tau_{i-1/i}(S)\}^2 + \{\tau_{i/i+1}(S+\Delta S)\}^2 \\ &- \{\tau_{i/i+1}(S)\}^2\big]\,dx\end{aligned} \tag{A7}$$

The shear stresses $\tau_{i-1/i}$ and $\tau_{i/i+1}$ were calculated by substituting Equations A1–A3 into Equation 1 for uncracked interfaces in Regions A and B, and by Equation 4 for the cracked "Nc"/"Nc + 1" interface in Region B. Then $\Delta U_{G,i}$ was calculated by Equation A7, from whose summation for $i = 1$ to N, the ΔU_G was calculated.

For the calculation of the G_d-value, Narin's method [1] was applied; for the two situations where the cracked area grows from S to $S + \Delta S_1$ and $S + \Delta S_2$, the corresponding values of $(W_p - \Delta U_e)/\Delta S$ were calculated. Then G_L-value was obtained by the linear extrapolation of these values to $\Delta S(\Delta d) = 0$ by Equation 14.

Acknowledgement

The authors wish to express their gratitude to The Ministry of Education, Science and Culture, Japan, for the grant-in-aid for scientific research No. 11555175.

References

1. J. J. BRENNAN and K. M. PREWO, *J. Mater. Sci.* **17** (1982) 2371.
2. K. M. PREWO, *ibid.* **21** (1986) 3590.
3. M. TAMURA, N. MIYAMOTO, M. SATO, O. SAKAMOTO and T. YAMAMURA, in *Proceedings of 1993 Powder Metallurgy World Congress*, 1993, p. 1350.
4. A. KUMAR and K. M. KNOWLES, *Acta Metall. Mater.* **44** (1996) 2901.
5. A. G. EVANS, M. Y. HE and J. W. HUTCHINSON, *J. Amer. Ceram. Soc.* **72** (1988) 2300.
6. M. D. THOULESS, O. SBAIZERO, L. SIGL and A. G. EVANS, *ibid.* **72** (1988) 525.
7. D. B. MARSHALL and A. G. EVANS, *ibid.* **68** (1985) 225.
8. H. H. SHIN and R. F. SPEYER, *J. Mater. Sci.* **29** (1994) 3630.
9. M. YATOMI, M. HOJO, M. TANAKA, S. OCHIAI, Y. SAWADA and J. TAKAHASI, *J. Soc. Mater. Sci., Japan* **47** (1998) 939.
10. J. M. HEDGEPETH, NASA TN D-882, Washington, 1961.
11. J. G. GOREE and R. S. GROSS, *Eng. Frac. Mech.* **13** (1980) 563.
12. L. R. DHARANI, W. F. JONES and J. G. GOREE, *ibid.* **17** (1983) 555.
13. J. A. NARIN, *J. Comp. Mater.* **22** (1988) 561.
14. S. OCHIAI, K. SCHULTE and P. W. M. PETERS, *Comp. Sci. Tech.* **44** (1991) 237.
15. S. OCHIAI, and M. HOJO, *J. Mater. Sci.* **31** (1996) 3861.
16. S. OCHIAI, M. HOJO, K. SCHULTE and B. FIEDLER, *Comp. Sci. Techn.* **57** (1997) 775.
17. S. OCHIAI, M. TANAKA and M. HOJO, *Comp. Interfaces* **5** (1998) 437.
18. N. F. DOW, G. E. C. Missile and Space Division, Report No. R63SD61, quoted by G. S. Holister and C. Thomas in Fiber Reinforced Materials (Elsevier, London, 1966), p. 23.

Received 29 July
and accepted 14 December 1999